13B.2

CIRRIFORM CLOUD OBSERVATION IN THE TROPICS BY VHF WIND PROFILER AND 95-GHz CLOUD RADAR

Masayuki K. YAMAMOTO*[1], Yuichi OHNO[2], Hajime OKAMOTO[3], Hiroaki HORIE[2], Kaori SATO[3], Noriyuki Nishi[4], Hiroshi KUMAGAI[2], Hajime NAGATA[1], Mamoru YAMAMOTO[1], Hiroyuki HASHIGUCHI[1], and Shoichiro FUKAO[1],

1. Research Institute for Sustainable Humanosphere, Kyoto University, Japan
2. National Institute of Information and Communications Technology, Japan
3. Center for Atmospheric and Oceanic Studies, Graduate School of Science, Tohoku University
4. Division of Earth and Planetary Sciences, Graduate School of Science, Kyoto University

1. Introduction

Cirriform clouds (cirrus, cirrostratus, cirrocumulus) existing in the upper part of the troposphere consist almost entirely of ice particles, and play a significant role in regulating the radiation balance of the earth-atmosphere system (Liou, 1986). Therefore, knowing of microphysical properties and dynamical processes related to them is important for parameterizing effects of cirriform clouds in numerical models. Particle falling velocity is one of crucial factors that determine lifetime of cirriform clouds, because it determines evaporation of cloud particles through sedimentation. The most unknown factor for observing correct particle falling velocity is vertical air velocity (hereafter V_{air}). Because means to directly observe V_{air} is limited, V_{air} is computed indirectly in most of the previous observations. Wind profiler operated at VHF frequency (VHF wind profiler), which directly observes vertical profiles of winds by receiving echoes from fluctuations of refractive index, is a useful instrument to directly observe V_{air} in and around cirriform clouds. In this extended abstract, it is shown that a combination of VHF wind profiler and millimeter-wave cloud profiling radar is a key tool to observe particle falling velocity in tropical cirriform clouds.

* Corresponding author address: Masayuki K. Yamamoto, Research Institute for Sustainable Humanosphere, Kyoto University, Gokasho, Uji, Kyoto 611-0011, Japan; e-mail: m-yamamo@rish.kyoto-u.ac.jp

2. DATA AND ANALYSIS METHOD

The Equatorial Atmosphere Radar (hereafter EAR) is a wind profiler operated at VHF frequency (47 MHz; radar wavelength of 6.38 m). The EAR has been operated at Equatorial Atmosphere Observatory, Kototabang, West Sumatra, Indonesia (0.2 degrees south, 100.32 degrees east, 865 m above mean sea level). For the system description of the EAR, see Fukao et al. (2003). During a period we focus on (14-15 November 2005), the EAR is operated by two observation modes; a standard mode to observe vertical and horizontal winds and an additional observation mode to steer radar beams only to the vertical direction, which contributes to an improvement of the estimation accuracy and data rate of V_{air} (hereafter vertical wind mode). We used V_{air} derived from the vertical wind mode. The vertical wind mode during 14-15 November 2005 is the same as used during 5-9 May 2004, except that a number of coherent integrations (N_{coh}) and FFT points (N_{FFT}) are changed to 64 and 1024, respectively (see Table 1 of Yamamoto et al. (2007)). For details of the vertical wind mode, see Yamamoto et al. (2007).

A 95-GHz cloud profiling radar (hereafter cloud radar) developed by National Institute of Information and Communications Technology (NICT), Japan observed radar reflectivity factor (hereafter Z_e) and Doppler velocity by receiving echoes from cloud particles. The cloud radar was temporarily operated at the Equatorial Atmosphere Observatory for the cirrus observation campaign. Doppler velocity was observed by pulse-pair method. For the system description of the cloud radar, see Horie et al. (2000).

Doppler velocity observed by the cloud radar (hereafter V_{air+Z}) is a sum of V_{air} and reflectivity-weighted particle falling velocity (hereafter V_Z; see Houze (1993) for its definition). Therefore V_Z is computed by subtracting V_{air} observed by the EAR from V_{air+Z}. Vertical profiles of V_{air} and V_Z are computed every 3 minutes, and further smoothed by 12-minute running average to reduce fluctuations in time. Vertical resolution used in data analysis is 150 m.

To investigate horizontal distribution of cumulus activity, equivalent blackbody brightness temperature (hereafter T_{BB}) observed by IR-1 (10.3-11.3 μm) channel of the weather satellite (MTSAT-1R) is used. Cloud-top altitudes were inferred by T_{BB} and vertical profile of temperature observed by radiosondes launched at the observation site during October-November 2005. T_{BB} is generally higher than real temperature at cloud top because clouds are not regarded as perfect black bodies (Sherwood et al., 2004); it means that cloud-top altitudes inferred from T_{BB} are generally lower than real cloud top, and indicate lowest altitudes where cloud top can exist.

3. RESULTS

3.1 Weather Satellite Observation

A case in the nighttime between 14 and 15 November 2005 is intensively studied. During the period, cirriform clouds in the outflow region of convective system were observed at the observation site. Figure1 shows T_{BB} from 2050 local standard time (hereafter LT) to 0650 LT. Note that LT is 7 hours earlier than universal time coordinated. After 20 LT, a region with T_{BB} of less than 205 K, which indicates that deep cumulus convection with cloud tops of higher than about 14.1 km, developed in the east and north of the observation site (Figures 1a-b). As deep cumulus convection develops over the observation site, cloud tops of higher than about 13.0 km, as indicated by T_{BB} of less than 215 K, began to cover the observation site. Around 00-01 LT, cloud tops of higher than about 15.4 km, as indicated by T_{BB} of less than 195 K, existed in the northeast of the observation site (Figure 1c). Clouds in an outflow region of convective system, as indicated by T_{BB} of less than 215 K, extended in the southeastward and covered the observation site (see Figures 1c-e). Around 06-07 LT, cloud tops observed over the observation site became lower than about 13.0 km (T_{BB} of greater than 215 K), as centers of cumulus convection moved to the east coastal region of Sumatra (Figure 1f).

3.2 Time-altitude variation of Z_e, V_{air+Z}, and V_{air}

The cloud radar observed echoes from cirriform clouds from 2030 LT 14 to 0730 LT 15 November 2005, as observed by the weather satellite (see Figures 1a-f and 2a). Echo tops observed by the cloud radar located above 12 km in most of the observation time, and reached to higher than 14 km from 2320LT 14 November to 0100 LT. Echo bottoms located around 8-10 km. V_{air+Z} generally shows consistent changes with Z_e; relatively smaller V_{air+Z} (and larger V_{air+Z} in amplitude) was observed for larger Z_e (see Figures 2a and b). Because Z_e is weighted by backscattering cross section which is proportional to the 6th power of particle effective diameter and hence generally have large values in the dominance of large-sized cloud particles, the observed feature in V_{air+Z} indicates that cloud particles with larger Z_e have larger particle falling velocity. Further, V_{air+Z} has consistent changes with V_{air}; V_{air+Z} of larger than -0.4 m/s (and smaller than 0.4 m/s in amplitude) tends to be found when upward (positive) V_{air} was observed. For example, this tendency is seen especially around 2140 LT and during 2340-2400 LT 14 November, and during 0240-0340 LT and 0420-0530 LT on 15 November. Further, V_{air+Z} showed vertically-standing feature in altitude throughout the observation period, while the vertically-standing feature is not seen in Z_e. In Section 3.3, a relationship between V_{air} and V_{air+Z} is investigated in detail.

3.3 Estimation of particle falling velocity using Doppler velocity observed by cloud profiling radar and vertical air velocity observed by VHF wind profiler

It is shown that direct V_{air} observation by VHF wind profiler is useful for deriving particle falling velocity. Firstly, relationships between V_{air} and V_{air+Z} are examined. Figure 3a shows a scatter plot between V_{air} and V_{air+Z} at 7.3-12.2 km, which is an altitude range that the cloud radar had a good data acquisition rate (higher than about 80 %) from 2000 LT 14 November to 0800 LT 15 November 2005. It is clear that V_{air+Z}, a sum of V_{air} and V_Z and was observed by the cloud radar, shows consistent changes with V_{air}. Figure 3b shows a scatter plot between V_{air} and V_z (= V_{air+Z} - V_{air}). Variations in V_z seem to have significant relationship with V_{air}; the correlation coefficient between V_{air} and V_z is only -0.01. These variations observed in V_z indicate that consistent changes between V_{air+Z} and V_{air} are caused by V_{air} component in V_{air+Z}.

Z_e is used as a proxy of cloud particle size to confirm that computed V_z shows a consistent change with cloud particle size. Figure 4a shows a scatter plot between V_{air+Z} and Z_e, both of which were observed by the cloud radar. A negative correlation between V_Z and Z_e, which indicates that cloud particles with relatively large size have larger falling velocity, is observed as previously shown in Figures 1a and b. However, V_{air+Z} contains large fluctuations for Z_e due to V_{air} changes in V_{air+Z}; the correlation coefficient between V_{air+Z} and Z_e is -0.46. Figure 4b shows a scatter plot between V_Z and Z_e. The correlation coefficient between V_Z and Z_e is -0.61, and shows a better correlation than between V_{air+Z} and Z_e. This improvement in the correlation coefficient indicates that the poorer correlation between V_{air+Z} and Z_e, as seen in Figure 3b, occurred due to upwelling and downwelling of V_{air}. Results shown in this section have demonstrated that V_{air} observation by VHF wind profiler is useful for observing particle falling velocity in cirriform clouds.

3.5 Comparison of particle falling velocity between the bottom and middle part of cirriform clouds.

By improving accuracy in deriving V_Z using VHF wind profiler, two different relationships between V_Z and Z_e were clearly observed between the middle part and the bottom part of the cirriform clouds. Figures 5a and b show scatter plots between V_Z and Z_e around bottom part (7.2-10.5 km) and middle part (10.5-12.2 km) of clouds, respectively. Changes of V_Z for Z_e in the bottom part are scattering as compared to ones in the middle part of clouds; the correlation coefficient between V_Z and Z_e at the bottom part is -0.55, and one at the middle part is -0.83. Because particle size distribution is a factor which determines both Z_e and V_Z, and particle shape is a factor which causes variability in V_Z, this scattering feature in the bottom part of clouds is explained by larger variability in particle size distribtion and particle shape.

Though changes of V_Z for Z_e are relatively scattering in the bottom part of clouds, a negative correlation between V_Z and Z_e is still observed; a regression line is computed to be Z_e = -77.9 V_z - 65.4 In the middle part of cloud, changes of V_Z for Z_e are realatively large; a regression line is computed to be Z_e = -31.9 V_z - 32.2. The larger negative slope in the bottom part than in the middle part indicates that relatively large-sized particles with a larger falling velocity dominantly exist in the bottom part of clouds.

4. SUMMARY

In the abstract, it has been demonstrated that a combination of VHF wind profiler and millimeter-wave cloud profiling radar is a key tool to observe particle falling velocity in tropical cirriform clouds. By improving the accuracy in deriving particle falling velocity, a clear difference in particle falling velocity between in the bottom and middle part of clouds has been shown. We hope that a capability of VHF wind profiler to observe vertical wind contributes to further understanding of microphysical and dynamical processes in cirriform clouds.

REFERENCES

Fukao, S., H. Hashiguchi, M. Yamamoto, T. Tsuda, T. Nakamura, M. K. Yamamoto, T. Sato, M. Hagio and Y. Yabugaki, 2003: The Equatorial Atmosphere Radar (EAR): System description and first results, *Radio Sci*., **38(3)**, 1053, doi:10.1029/2002RS002726.

Horie, H., T. Iguchi, H. Hanado, H. Kuroiwa, H. Okamoto and H. Kumagai, 2000: Development of a 95-GHz airborne cloud profiling radar (SPIDER) - Technical aspects -, *IEICE Trans. Commun.*, **E83-B(9)**, 2010-2020, 2000.

Houze, R. A., Jr., 1993: Cloud dynamics, 121 pp., Academic, San Diego, Calif.

Liou, K.-N., 1986: Influence of cirrus clouds on weather and climate processes: A global perspective, *Mon. Wea. Rev.*, **114**, 1167-1199.

Sherwood, S. C., P. Minnis, and M. McGill, 2004: Deep convective cloud-top heights and their thermodynamic control during CRYSTAL-FACE, *J. Geophys. Res.*, **109**, D20119, doi:10.1029/2004JD004811.

Yamamoto, M. K., N. Nishi, T. Horinouchi, M. Niwano, and S. Fukao, Vertical wind observation in the tropical upper troposphere by VHF wind profiler: A case study, *Radio Sci.*, **42**, RS3005, doi:10.1029/2006RS003538.

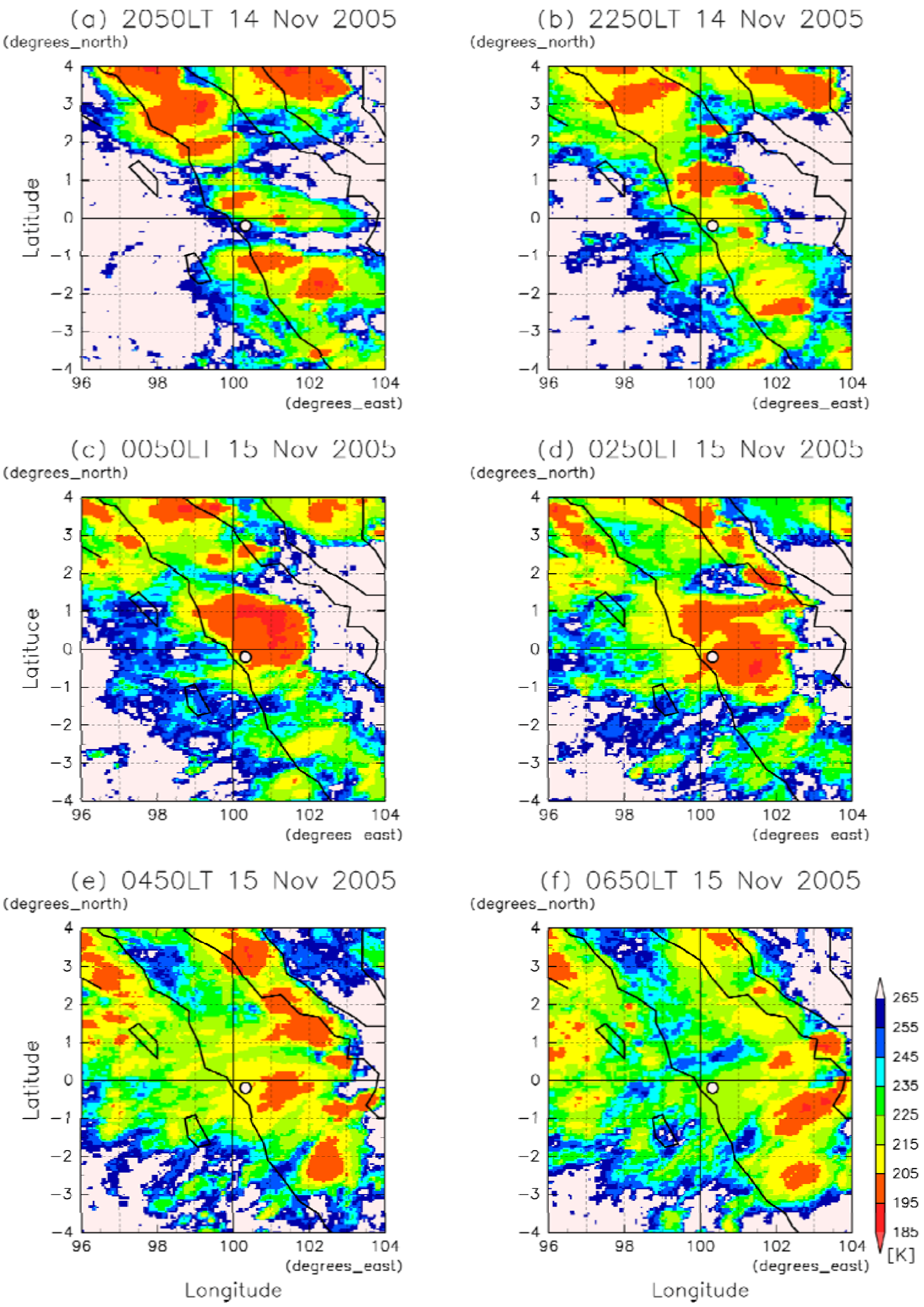

Figure 1. Longitude-latitude plots of T_{BB} observed by the IR-1 channel of MTSAT-1R . Contours are plotted with an interval of two hours from 2050 LT 14 to 0650 LT 15 Novemver 2005. Circles in each panel indicate the location of the observation site (0.2 degrees south, 100.32 degrees east, 865 m above mean sea level). Solid curves show coastlines.

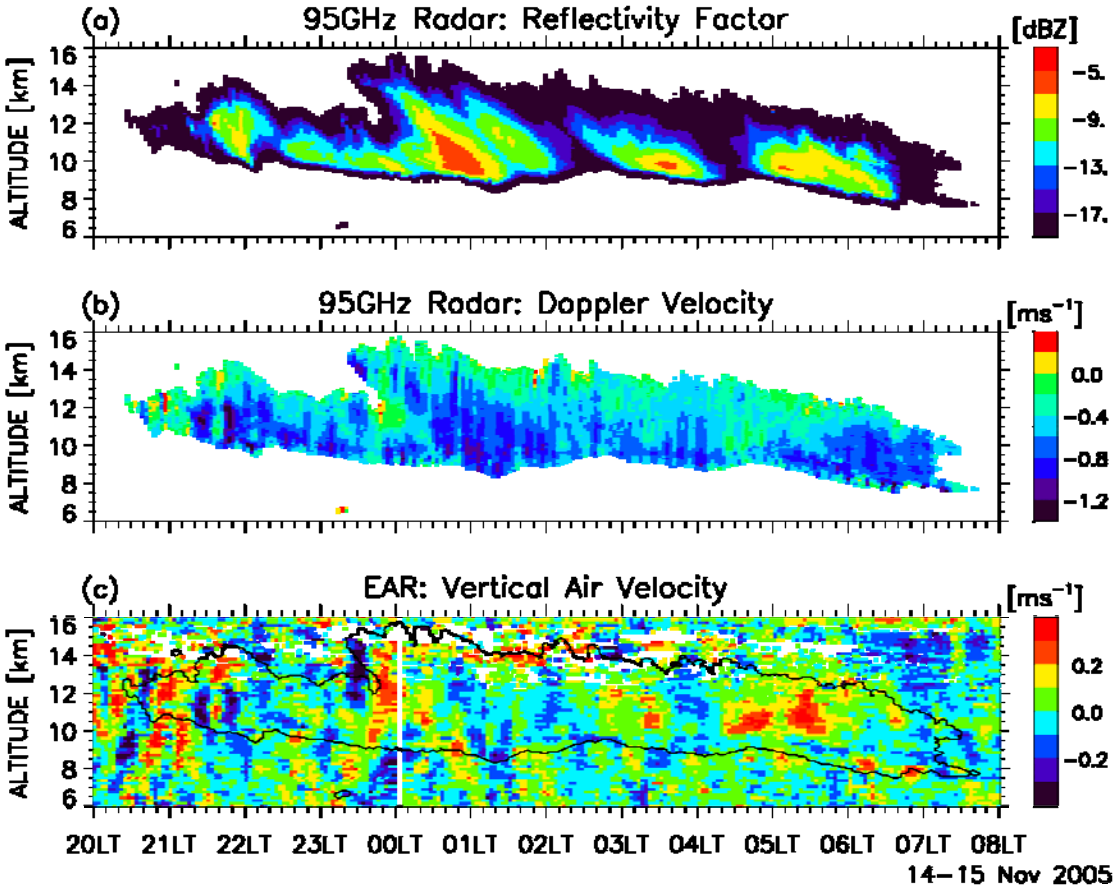

Figure 2. Time-altitude plots of (a) Z_e, (b) V_{air+Z}, and (c) V_{air} from 2000 LT 14 to 0800 LT 15 November 2005. Solid contour in panel (c) indicates the region where the cloud radar received echoes from cloud particles.

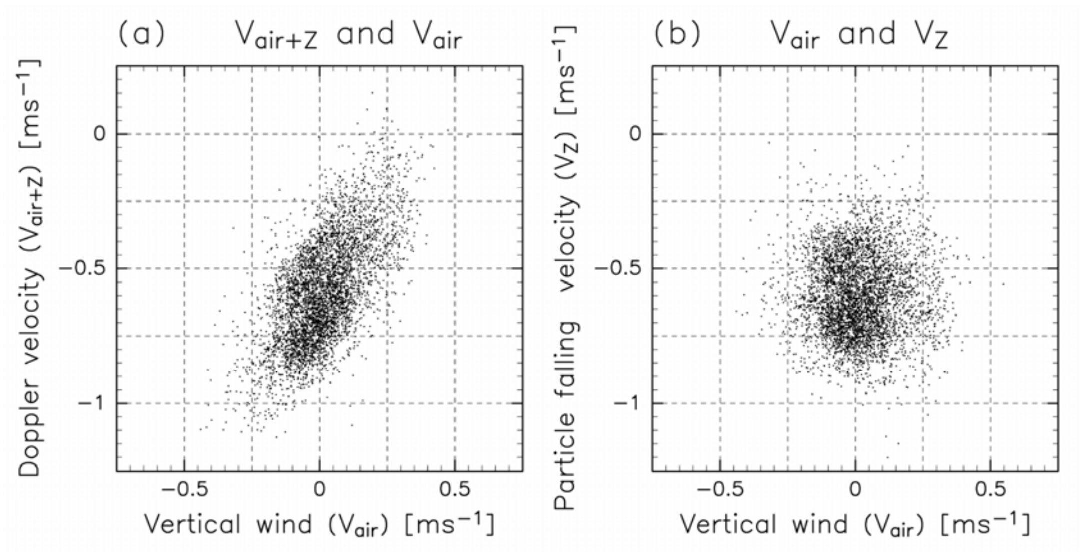

Figure 3. Scatter plot between (a) V_{air} and V_{air+Z}, and (b) V_{air} and V_z at 7.2-12.2 km from 2000 LT 14 to 0800 LT 15 November 2005.

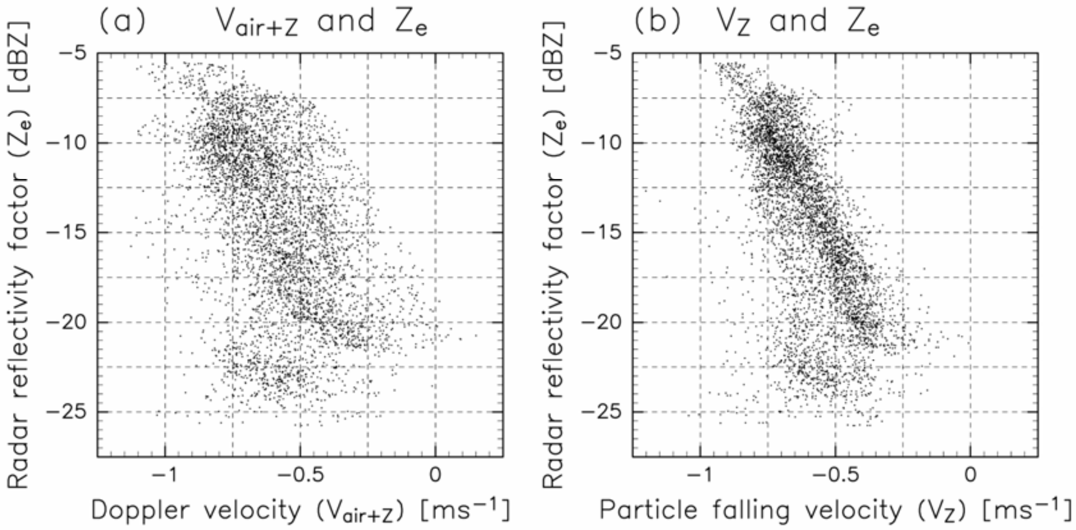

Figure 4. Scatter plot between (a) V_{air+Z} and Z_e, and (b) V_z and Z_e at 7.2-12.2 km from 2000 LT 14 to 0800 LT 15 November 2005.

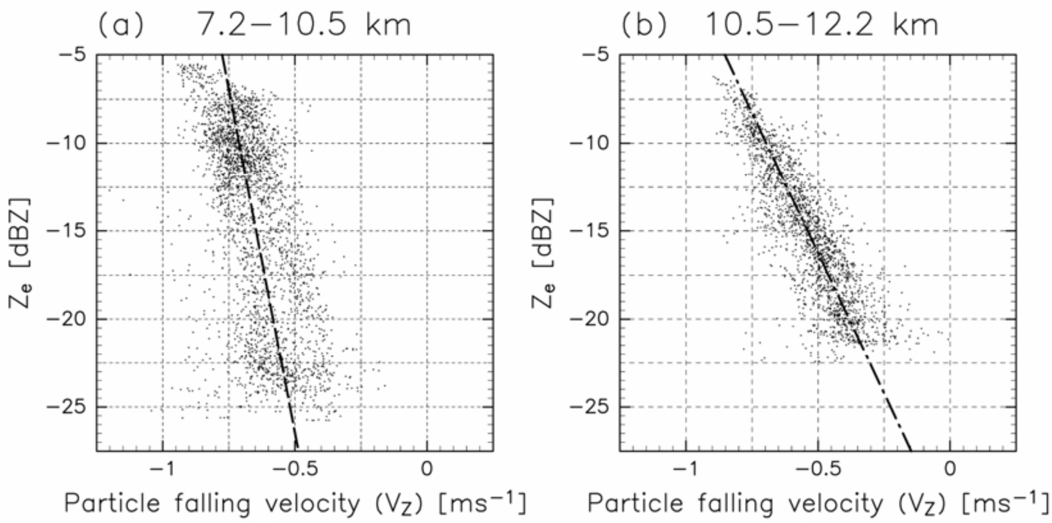

Figure 5. Scatter plot between (a) V_Z and Z_e at 7.2-10.5 km, and (b) V_z and Z_e at 10.5-12.2 km from 2000 LT 14 to 0800 LT 15 November 2005. Broken line in panel (a) and dash-dotted line in panel (b) show regression lines computed in the ranges of 7.2-10.5 km (broken line; Z_e = -77.9 V_z - 65.4), and 10.5-12.2 km (dash-dotted line; Z_e = -31.9 V_z - 32.2), respectively.